Journal of
Materials Chemistry C

ROYAL SOCIETY OF CHEMISTRY

PAPER

View Article Online
View Journal

Cite this: DOI: 10.1039/d2tc00486k

Inherent electron and hole trapping in amorphous phase-change memory materials: $Ge_2Sb_2Te_5$

Konstantinos Konstantinou, *[a] Stephen R. Elliott [b] and Jaakko Akola [ac]

Received 3rd February 2022,
Accepted 1st April 2022

DOI: 10.1039/d2tc00486k

rsc.li/materials-c

While the amorphous state of a chalcogenide phase-change material is formed inside an electronic-memory device *via* Joule heating, caused by an applied voltage pulse, it is in the presence of excess field-induced electrons and holes. Here, hybrid density-functional-theory calculations for glassy $Ge_2Sb_2Te_5$ demonstrate that extra electrons are trapped spontaneously, creating deep traps in the band gap. Hole self-trapping is also energetically favourable, producing states around midgap. The traps have a relatively low ionization energy, indicating that they can easily be thermally released. Near-linear triatomic Te–Ge/Sb–Te/Ge/Sb environments are the structural motifs where the extra electrons/holes are trapped inside the glass network, highlighting that the intrinsic axial bonds of octahedral-like sites in amorphous $Ge_2Sb_2Te_5$ can serve as charge-trapping centres. Trapping of two electrons in a chain-like structure of connected triads results in breaking of some of these highly polarizable long bonds. These results establish the foundations of the origin of charge trapping in amorphous phase-change materials, and they may have important implications for our understanding of resistance drift in electronic-memory devices and of electronic-excitation-induced athermal melting.

Open Access Article. Published on 06 April 2022. Downloaded on 4/8/2022 12:18:25 PM.
This article is licensed under a Creative Commons Attribution 3.0 Unported Licence.

1. Introduction

The lack of long-range order in amorphous (glassy) materials serves as a natural cause for the formation of spatially localized electronic states in the band gap.[1] Structural disorder facilitates charge trapping in a glassy structure by creating precursor sites and allowing for relaxation of the local atomic environment.[2] At some of these sites, carriers can be trapped spontaneously, whereas trapping at others requires the carrier to overcome an energy barrier.[3] Intrinsic electron and hole trapping in amorphous oxide semiconductors has been demonstrated by theoretical calculations.[4–9] Usually, shallow electronic states near the bottom of the conduction band or the top of the valence band can serve as charge-trapping centres, while deep-trap states have been reported, as well, in some amorphous models.[10,11]

Phase-change memory materials based on chalcogenide alloys encode stored digital binary data as metastable structural states of the material.[12] In non-volatile phase-change random-access electronic/optical memory (PCRAM) devices, Joule heating results in ultra-fast, reversible transformations between a semiconducting electrically-resistive amorphous state and a degenerate semiconducting electrically-conductive crystalline state, respectively, caused by applied voltage/laser write pulses.[13] Typically, glass formation involves quenching of a liquid which is created by the external thermal melting of a crystal (melt-and-quench process). However, in PCRAM devices, the glassy state of the chalcogenide material is made in a distinctive way during the *RESET* process. The thermal energy for melting the memory material in a PCRAM cell is provided internally by the Joule heating associated with the application of the *RESET* voltage pulse. The current–voltage characteristics of the memory material are non-linear, especially in the glassy state, and the non-Ohmic increase in current is due to electric-field-assisted-carrier generation processes.[14,15] The electron/hole current density, that is produced by the *RESET* pulse, is rather high inside the PCRAM cell before the amorphous state of the memory material is generated on quenching from the liquid. Under such conditions, intrinsic electron and hole trapping in the localized states of the liquid, and then the glassy material should be expected, leading to the creation of charge-trapping centres in the band gap of the glass.[16]

The electrical resistance of the amorphous phase in a PCRAM cell increases (''drifts'') with time following a power law, which increases the memory window in time, but it corresponds to an obstacle for the implementation of multi-bit storage, multi-level programming operations in PCRAM devices.[17] The time-dependent resistance-drift issue in phase-change materials has been mainly ascribed to structural

[a] *Computational Physics Laboratory, Faculty of Engineering and Natural Sciences, Tampere University, Tampere FI-33014, Finland. E-mail: konstantinos.konstantinou@tuni.fi*
[b] *Physical and Theoretical Chemistry Laboratory, University of Oxford, Oxford OX1 3QZ, UK*
[c] *Department of Physics, Norwegian University of Science and Technology (NTNU), Trondheim NO-7491, Norway*

Open Access Article. Published on 06 April 2022. Downloaded on 4/8/2022 12:18:25 PM.
This article is licensed under a Creative Commons Attribution 3.0 Unported Licence.

relaxation of the glassy state.[18–24] However, the concept of charge trapping has been recently employed in two different studies to explain resistance drift in melt-quenched phase-change materials at room temperature and below.[25,26]

Photo-excitation experiments have suggested that trapping and de-trapping of charges can give rise to changes in the current–voltage characteristics of the memory material.[25] The authors argued that the gradual ionization of the electron traps over time leads to an increase of the potential barrier needed to be overcome by the holes at the contact between electrode and phase-change memory material, providing an explanation for resistance drift.[25] An electronic-flavoured mechanism for understanding resistance drift was also proposed theoretically, based on the slow deep-trap release and recombination of charge carriers.[26] In this model, following electron/hole injection during the *RESET* process in a PCRAM cell, thermally de-trapped electrons can recombine with the thermally generated holes in the valence band, which, therefore, reduces the number of free charge carriers in the amorphous state of the memory material.[26] This effect contributes to the measured current in the PCRAM device, and it can be considered to be responsible for the drift observed in the resistance of the glass.

It has been reported from experimental studies[27–29] and atomistic simulations[22,30–33] that several localized unoccupied and occupied electronic states exist in the vicinity of the band gap in amorphous phase-change materials. Defect-related mid-gap electronic states in glassy models of $Ge_2Sb_2Te_5$ were found to be able to capture electrons, leading to the creation of deep-trap electron centres in the conduction band of the chalcogenide material.[31] Hence, these simulations provided an indication about charge trapping in amorphous phase-change memory materials. In addition, localized electronic states were identified in the tails of the conduction and valence bands of the amorphous models, which can give rise to possible charge-trapping sites.

Modelling of charge (electron and hole) localization in amorphous solids provides a strong stimulus for performing atomistic simulations. In this study, we aim to achieve a fundamental understanding, at the atomistic level, of charge trapping in phase-change memory materials during the electron-/hole-injection process accompanying the *RESET* process and generation of the glass. We reveal how spontaneous electron and hole localization in the conduction- and valence-band tails leads to the creation of self-trapping centres, demonstrating that charge trapping corresponds to an intrinsic property of the chalcogenide glassy material. In addition, we identify the structural fingerprints for electron-/hole-trapping sites in amorphous phase-change materials, show the impact of charge trapping on the atomic bonding of these materials, and discuss implications related to the memory-device operation.

2. Computational methods

2.1 Model structures

A study of modelling defects in amorphous materials should involve a statistical analysis of many different models in order to investigate the probability of defect formation and to obtain distributions of their properties. The machine-learned Gaussian Approximation Potential (GAP) developed for Ge–Sb–Te materials[34] was employed to generate an ensemble of periodic models of amorphous $Ge_2Sb_2Te_5$ (GST-225), each containing 315 atoms, using classical molecular-dynamics (MD) simulations and by following a melt-and-quench approach. Density-functional theory (DFT) calculations were then used to further optimize the atomic geometry of the modelled glassy systems and to obtain their electronic structures. Details about these simulations and the quality of the generated amorphous models can be found in ref. 31. In this study, seventeen (17) independent models of amorphous GST-225 were selected from the ensemble database to simulate charge trapping to obtain a statistical understanding about the potential trapping sites in the memory material. It should be noted that these model structures correspond to glass models that were selected not to contain defect-related electronic states inside the band gap (see Supplementary Table 1 in ref. 31), in order to focus on the investigation of charge-trapping processes only at the conduction- and valence-band edges of the amorphous models.

Further, to increase the statistical significance of our simulations, we also performed electron- and hole-trapping calculations in a melt–quenched amorphous GST-225 model of 460 atoms generated by *ab initio* (DFT) MD simulation.[35] It is important to highlight that this glassy model was not part of the training-set structures used to develop the GAP potential employed to generate the rest of the glassy models used in this study. Moreover, a 648-atom ''as-deposited'' amorphous structure of GST-225, generated by DFT-MD simulation,[36] was also used to investigate charge-trapping processes in a ''vapour-created'' amorphous model.

2.2 Electronic-structure calculations

Electron- and hole-trapping events were modelled by injecting an extra electron and hole, respectively, in the relaxed ground state of each glass structure and then minimizing the energy with respect to the atomic coordinates. Along with the extra electron/hole, a compensating background positive/negative charge, that is uniform across the simulation cell, was included in each case. Moreover, double-charge trapping was also investigated by adding a second electron (hole) to the existing single-electron (hole) trapped model structures and then re-optimizing their geometries. The geometry optimizations were performed using DFT as implemented in the CP2K code,[37] which employs a mixed Gaussian basis set with an auxiliary plane-wave basis set to represent the electrons in the modelled system.[38] A molecularly-optimized double-ζ valence-polarized (DZVP) Gaussian basis set[39] was used for all atomic species, in conjunction with the Goedecker–Teter–Hutter (GTH) pseudopotential.[40] The plane-wave energy cut-off was set to 5440 eV (400 Ry). The range-separated hybrid PBE0 functional[41] was used in all calculations, with a cut-off radius of 3 Å for the truncated Coulomb operator. The inclusion of the Hartree–Fock exchange provides a more accurate description of the band gap and the localized electronic states that are potentially

This journal is © The Royal Society of Chemistry 2022

Open Access Article. Published on 06 April 2022. Downloaded on 4/8/2022 12:18:25 PM.
This article is licensed under a Creative Commons Attribution 3.0 Unported Licence.

involved in charge-trapping events in our modelled glassy structures.[31,42] The computational cost of hybrid-functional calculations was reduced by using the auxiliary density-matrix method (ADMM).[43] The Broyden–Fletcher–Goldfarb–Shanno (BFGS) algorithm was applied in the geometry optimizations and the forces on individual atoms were minimized to below 0.023 eV $Å^{-1}$ (4.5×10^{-4} Hartree $Bohr^{-1}$).

3. Results and discussion

3.1 Electron and hole traps

The electronic-structure calculations predict an average Kohn–Sham (KS) band gap of ∼0.65 eV for the 315-atom GAP-MD amorphous models, ranging between 0.55 and 0.75 eV. The KS band gaps for the relaxed ground state of the DFT-MD melt–quenched and as-deposited GST-225 model structures were found to be 0.69 eV and 0.66 eV, respectively (see Fig. 1a for the total electronic densities of states around the Fermi level). These calculated values of the band gap agree very well with the experimentally reported values for amorphous GST-225, ranging between 0.6 and 0.8 eV,[44,45] as well as with previous modelling studies.[30,42]

An extra electron added to the glass model occupies the LUMO (lowest unoccupied molecular orbital) at the bottom of the conduction band of the neutral system. Hence, electron trapping produces occupied states in the band gap. The average position of the KS level, for all the amorphous models studied here, for the electron traps is ∼0.58 eV below the bottom of the conduction band, which, considering the size of the band gap of the glass, corresponds to deep traps in the electronic structure of the GST-225 models. The distribution of the KS levels for the electron-trapping events is shown in Fig. 1b. Correspondingly, an extra hole added to the neutral structure will be potentially localized at the top of the valence band in the HOMO (highest occupied molecular orbital) of the system. It was found that hole trapping produces unoccupied states in the band gap of the amorphous models, while the average position of the KS level for the hole traps is ∼0.37 eV above the top of the valence band (see Fig. 1b for the distribution of the KS levels for the hole trapping).

The total and partial electronic densities of states (DOS, PDOS, respectively) of the GST-225 glass model generated by a

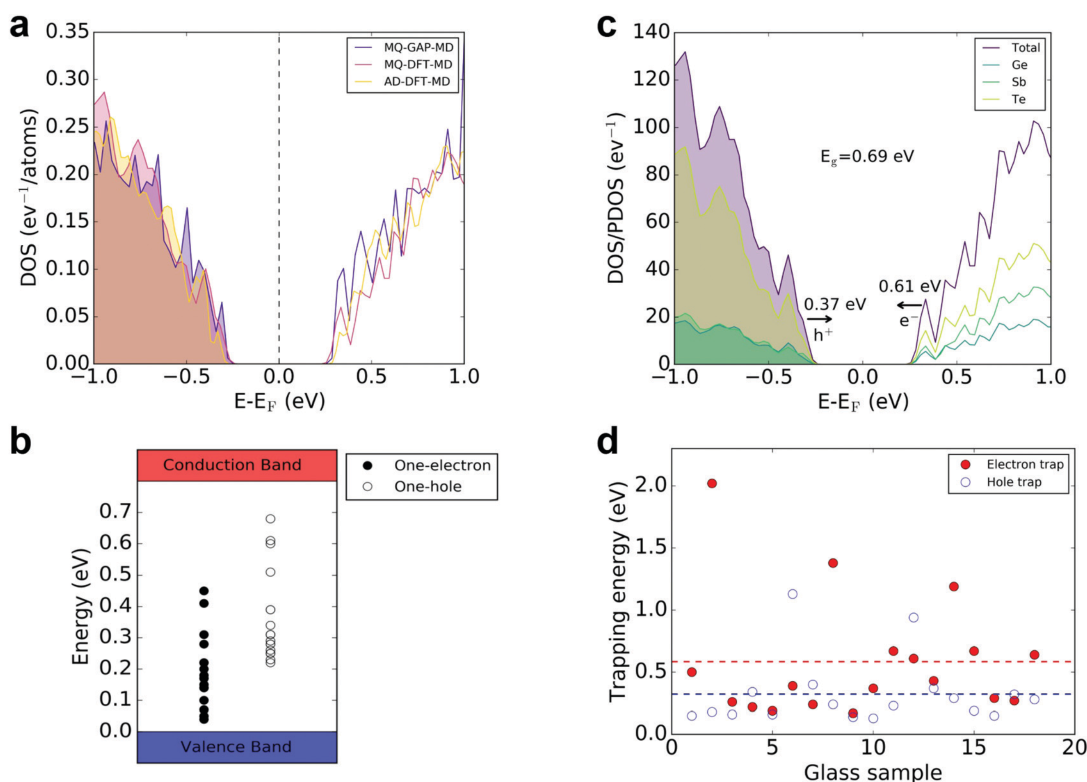

Fig. 1 (a) Total electronic densities of states (DOS) near the top of the valence band and the bottom of the conduction band of glassy GST-225 models generated with melt-and-quench GAP-MD (sample #3 from ref. 31), melt-and-quench DFT-MD,[35] and as-deposited DFT-MD[36] simulations. (b) Distributions of the Kohn–Sham levels for the electron- and hole-trapping events in the amorphous GST-225 model structures. (c) Total and partial electronic densities of states (DOS/PDOS) of the amorphous GST-225 model generated with a melt-and-quench DFT-MD simulation. A hybrid-functional electronic-structure calculation results in a HOMO–LUMO Kohn–Sham band gap, E_g, of 0.69 eV for the relaxed ground state of the neutral system. An extra electron (e^-) occupies the LUMO electronic state, and this state shifts by 0.61 eV towards the valence-band maximum following geometry relaxation, as indicated by the relevant arrow. An extra hole (h^+) is localized in the HOMO electronic state, and it produces an unoccupied state at an energy level of 0.37 eV above the top of the valence band, as indicated by the respective arrow. (d) Distributions of the calculated electron- and hole-trapping energies for all the simulated glassy structures.

Open Access Article. Published on 06 April 2022. Downloaded on 4/8/2022 12:18:25 PM.
This article is licensed under a Creative Commons Attribution 3.0 Unported Licence.

melt-and-quench DFT-MD simulation are shown in Fig. 1c. An extra electron (e^-) was added to the relaxed ground state of the amorphous model, and the geometry of the glass structure was then re-optimized with a hybrid-DFT calculation. The LUMO electronic state, at the bottom of the conduction band, becomes an occupied molecular orbital, and the energy position of this state is 0.61 eV below the conduction-band minimum, located very close to the top of the valence band, and hence indicating a deep electron trap. The addition of an extra hole (h^+) in the relaxed ground state of the neutral system results, after a geometry optimization, in the creation of an unoccupied electronic state, located around midgap, at an energy position of 0.37 eV above the valence-band maximum.

The simulations indicate that electrons and holes are trapped spontaneously within the amorphous network of GST-225, without needing to overcome an activation barrier. The electron-trapping energies were calculated as the energy difference between the total energy of the glass structure with the extra electron in the neutral geometry (*i.e.* before geometry optimization) and the total energy of the fully relaxed glass structure with the extra, self-trapped electron. The calculations show an average electron-trapping energy of $\sim$0.57 eV, with a wide distribution ranging between 0.17 and 2.0 eV (see Fig. 1d). The positive values of trapping energies indicate that spontaneous electron trapping is energetically favourable in the GST-225 amorphous structures. The trapping energies for holes were calculated in a similar way to that for the electrons described above. The calculations show an average hole-trapping energy of $\sim$0.32 eV, ranging between 0.13 and 1.13 eV (see Fig. 1d). Again, the positive values of trapping energies indicate that hole self-trapping is also energetically favourable in the model GST-225 systems.

In addition, the electron-/hole-trapping energies can give a lower limit for thermal-ionization energies of trapped electrons and holes. The calculated energies suggest that most of these electron and hole centres, generated in the GST-225 model structures studied here, will be relatively stable at room temperature. Nevertheless, the low calculated values of some of these trapping energies indicate that only a small amount of energy is needed to thermally release electrons and holes from these traps. Considering the deep one-electron traps in the band gap of amorphous GST-225, a potential thermal release of an electron from such a trap state could be beneficial for a recombination with thermally generated holes in the valence band. Correspondingly, a potential thermal release of a hole from the one-hole traps could lead to recombination with electrons in the (unoccupied) mid-gap states that exist in the band gap of glassy GST-225.[31] This observation supports the view proposed about time-dependent resistance-drift in amorphous phase-change materials, which entails charge release from traps with a range of trapping energies contributing to the measured current after a *RESET* voltage pulse. Correspondingly, this can be interpreted as a resistance change in the glassy phase of the memory material.[26]

It should be noted that the initial electron/hole states are already partially localized in the neutral geometry of the simulated structure, but the degree of spatial localization varies among different models of amorphous GST-225. This can affect the calculated trapping energies, since a larger difference in the degree of spatial localization, before and after the geometry relaxation of the glass structure with an extra electron/hole, results in a higher kinetic-energy cost upon localization.[2,3,8,9] Considering the electron and hole mobility edges, which are located deeper in the bands with respect to the conduction-band minimum and valence-band maximum, respectively, this would reduce the computed values of the trapping energies. Such an effect would strengthen the argument of possible charge release at room temperature and/or higher temperatures. However, we note that the dynamics of electron/hole de-trapping should be determined explicitly to quantify the temperature-dependent behaviour of charge release inside the amorphous structure.

3.2 Local atomic environments of charge-trapping sites

An analysis of the spin-density distribution for the glass models with an extra electron (hole) reveals the structural motifs in the amorphous GST-225 models responsible for the charge trapping. The calculations indicate that the extra electrons and holes show a preference for localization in defective octahedral sites within the glassy network. In particular, the near-linear triatomic environments in "see-saw" 4-coordinated or 5-coordinated (and more rarely 6-coordinated) configurations serve as the structural precursor for charge trapping in the glassy model structures. An example of an electron trap in one of the amorphous structures is shown in Fig. 2a. The extra electron is localized on a 4-coordinated Ge atom in a "see-saw" configuration, where there is a Te–Ge–Te environment with a near-linear bond angle of 156.6° (Fig. 2b).

Among the simulated structures, electron trapping was also found to occur in a configuration where two such triatomic environments are connected, forming a 5-membered, almost-linear chain, as shown in Fig. 2c and d. A Te–Ge–Te structural motif with a 140.3° angle is connected to another near-linear Te–Ge–Te triad with an angle of 165.2°, forming a continuous chain where the electron is trapped, in one of the GST-225 glass models generated by GAP-MD simulations (Fig. 2c). In the DFT-MD melt-and-quench model structure, a Te–Ge–Te and a Te–Sb–Sb environment with 153.8° and 168.6° angles, respectively, are connected to create a chain-like structure, which similarly traps the extra electron (Fig. 2d).

Examples of hole traps in five different melt-and-quench-generated simulated structures and the as-deposited-generated amorphous model are shown in Fig. 3. Te–Ge–Te triads, with angles of 158.2° and 173.1°, associated with "see-saw" 4-coordinated Ge atoms, trap holes spontaneously inside the glass structure (Fig. 3a and b). In addition, Te–Sb–Te and Te–Ge–Te triatomic environments with wide angles of 159.7° and 166.1°, respectively, associated with 5-coordinated Sb (Fig. 3c) and Ge (Fig. 3d) atoms, have been identified as potential hole-trapping sites inside the GST-225 models. Moreover, two connected triads can form a chain-like motif that is able to trap holes, as can be seen in Fig. 3e, where a Te–Sb–Te environment

Open Access Article. Published on 06 April 2022. Downloaded on 4/8/2022 12:18:25 PM. This article is licensed under a Creative Commons Attribution 3.0 Unported Licence.

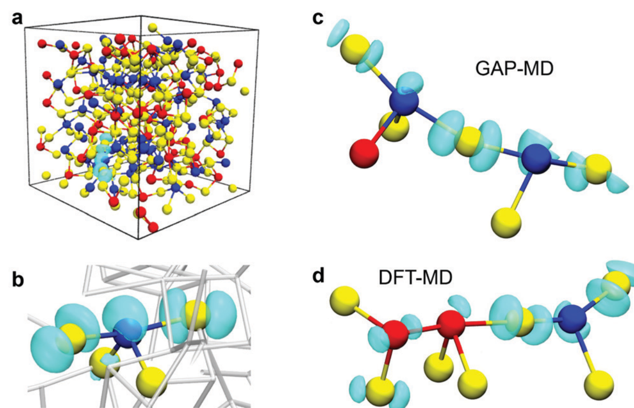

Fig. 2 (a) Spin-density distribution and atomic geometry of an intrinsic electron trap in a GST-225 glass model (#7 from ref. 31). (b) The extra electron is well localized on a wide-angle, almost-linear Te–Ge–Te triatomic environment in a defective octahedral-like "see-saw" configuration. Spin-density distribution and atomic geometry of two other intrinsic electron traps in GST-225 glass models generated with melt-and-quench simulations: (c) GAP-MD (sample #19 from ref. 31) and (d) DFT-MD.[35] Two connected near-linear triatomic environments form a 5-membered chain-like Te–Ge/Sb–Te/Ge/Sb structural motif that hosts the extra electron in the amorphous models. Ge atoms are blue, Sb are red, and Te are yellow. In panel (b), the atomic bonds in the rest of the amorphous network are rendered in grey. In every configuration, the iso-value of the spin density (cyan iso-surface) is equal to 0.002 e Å^{-3}.

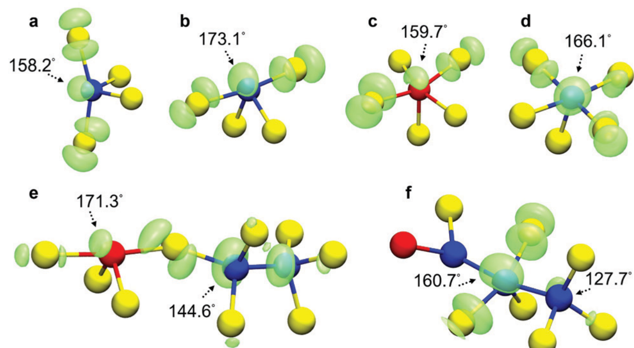

Fig. 3 Spin-density distribution and atomic geometry of representative intrinsic hole traps in five different melt-and-quench-generated GST-225 glass models: (a) #1, (b) #10, (c) #17, (d) #27 and (e) #21 from ref. 31 and (f) the as-deposited-generated amorphous GST-225 structure.[36] Wide-angle, almost-linear Te–Ge/Sb–Te triatomic geometries from "see-saw" 4-coordinated and 5-coordinated configurations are associated with the hole localization. Two connected triads can create a chain-like hole-trapping site inside the amorphous network. Despite the increased amount of tetrahedral Ge atoms and homopolar bonds, the hole localization in the as-deposited model structure is still associated with a near-linear Te–Ge–Te triatomic environment from a 5-coordinated configuration. Ge atoms are blue, Sb are red, and Te are yellow. In every configuration, the iso-value of the spin density (green iso-surface) is equal to 0.002 e Å^{-3}.

with a 171.3° angle and a Te–Ge–Ge environment with a 144.6° angle, from two different 4-coordinated Sb and Ge atoms, create the structure that hosts the extra hole trapped in the glass model.

It has been previously reported that the as-deposited amorphous GST-225 simulated structure differs geometrically from a melt–quench-generated glassy model.[36] In particular, it was demonstrated that, in the as-deposited amorphous network, Ge atoms show a preference for tetrahedral local environments, while the amount of homopolar bonds is larger (*i.e.* a reduced number of near-linear configurations) compared to the melt–quench structure.[36] From the calculations performed here for the as-deposited GST-225 model, it was found that an extra hole is localized on a Te–Ge–Te triatomic environment with a bond angle of 160.7°, associated with a 5-coordinated Ge atom (Fig. 3f), highlighting, despite the prominent overall differences in the local atomic structure, that the defective octahedral-like environments are instrumental for the charge-trapping processes inside the amorphous GST-225 material.

From a geometric point of view, the bond-angle distribution (BAD) can provide information about the relevant local atomic environments inside the glass structure through a description of the statistics of angle formation between the respective species within the amorphous network. The partial BAD functions for different types of triads of atoms in the GST-225 amorphous structure were calculated for all the glass models studied here and are shown, averaged, in Fig. 4. In this analysis, we consider that a bond exists between two atoms if the interatomic distance between them is equal to or smaller than the cut-off given to describe the maximum distance for nearest-neighbour atoms between the relating species within their first coordination shell (*i.e.* local atomic coordination). In our study, we applied a uniform geometric bond cut-off distance of 3.2 Å for all pairs of atomic species. We note that this is a value that has been previously used in several modelling studies of amorphous GST-225,[30,35,46,47] while it has also been demonstrated that it provides local coordination environments in

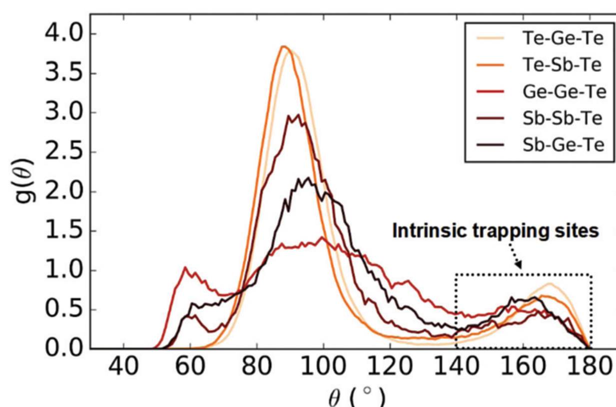

Fig. 4 Partial bond–angle distributions for different types of triatomic configurations, having Ge or Sb as the central atom, calculated as averages for all the GST-225 simulated glass structures. The peak at a bond angle of ~169° is indicative of the near-linear (axial) arrangements of chemically ordered triads, from defective octahedral-like atomic geometries, that were found to trap electrons and holes in the model structures. Local environments with a range of wide angles between 140° and 180° (shown inside the black dashed frame) provide a broad source of potential charge-trapping sites inside the amorphous network of GST-225. A uniform nearest-neighbour (bond) cut-off distance of 3.2 Å was used for all the pairs of atomic species to calculate the bond-angle distributions.

good agreement with analyses from other, DFT-related methods (*e.g.* by using the Electron-Localization Function).[31,34,48]

The first peak at a bond angle of $\sim 60^\circ$ is indicative of the presence of some triangular configurations inside the amorphous network. The main peak at a bond angle of $\sim 90^\circ$ corresponds to defective-octahedral local environments, which are predominantly formed in amorphous phase-change memory materials.[34] The third peak at a bond angle of $\sim 169^\circ$ corresponds to the axial configurations in defective octahedral environments, highlighting the presence of these near-linear geometries of triads of atoms in the glassy phase of GST-225. It can be observed that this peak is mainly due to near-linear arrangements of chemically ordered Te–Ge/Sb–Te triads, which are the environments that were found to be responsible for electron/hole trapping in the modelled systems. Moreover, the tails of the BAD distributions span between 140° and 180°, for several combinations of atomic species, providing a range of local environments with wide angles inside the glass as potential sites for charge trapping. Bond-angle distributions typical of distorted octahedral-like atomic geometries (*i.e.* a strong maximum at $\sim 90^\circ$ and a smaller peak in the region around $\sim 170^\circ$) have been reported in melt-and-quenched amorphous models of phase-change materials generated by DFT-MD simulations for GST-225[30,35,46–48] and Sb_2Te_3,[49,50] a neural-network interatomic potential for GeTe,[51] and GAP-MD simulations for GST-225[34] and Sb_2Te_3,[50] as well as in a quench-rate and size-dependent study for GST-225.[52]

Electron-polarized linear atomic chains have been previously proposed to be a characteristic structural feature in amorphous phase-change materials.[53] It was found that a large proportion of 3-membered chains (*i.e.* linear arrangements of triatomic configurations) exist inside the glass network, while a small amount of 4- and 5-membered chains were also identified in the simulated structure of glassy GST-225.[53] Near-linear atomic chains were also found to be a prevailing geometric structural pattern in amorphous Sb_2Te_3.[33] It was shown that atoms in near-linear chains comprise approximately half of the amorphous structure, while the statistics from the chain analysis highlighted that triatomic, almost-linear environments are the predominant structural motif.[33] In addition, electron localization of the LUMO state at the bottom of the conduction band has been associated with such chain-like structures in previous simulation studies of amorphous GST-225[30] and Sb_2Te_3.[33]

We note that amorphous GST-225 models generated with the GAP potential can have a reduced amount of tetrahedral Ge configurations in the simulated structure, compared to DFT-generated models, as we have discussed in our previous studies.[31,34] However, in this study, our independent calculations for purely DFT-MD-generated amorphous models, which were not even part of the GAP training-set configurations, showed that the Ge tetrahedral environments are not involved in the charge-trapping processes; therefore, any possible slight underestimation of those configurations in the GAP models should not affect the substance of our observations, relating to the intrinsic trapping sites inside the glassy GST-225 material.

3.3 Double electron/hole trapping

The interaction between localized electrons (holes) can lead to the formation of doubly-charged trapped states inside the material. Double-hole traps have been suggested in transition-metal oxides[54] and amorphous TiO_2,[9] while the existence of double-electron traps was predicted in amorphous models of SiO_2[55] and HfO_2[11] from theoretical calculations. In this study, the possibility of double-charge trapping in the glassy models of GST-225 was investigated by adding an extra electron/hole to the existing single electron/hole trapped structures.

It was found that the addition of the second electron facilitates the creation of a deeper singlet occupied KS state in the band gap of the amorphous models compared to the one-electron traps, located, on average, at 0.63 eV below the bottom of the conduction band. Correspondingly, the double-hole traps create unoccupied KS states in the band gap of the glass, with an average position of 0.51 eV above the top of the valence band, considerably deeper compared to the one-hole trapped systems. A similar trend was found for double-charge trapping in oxide glasses[11,55] and other ionic systems.[56] In addition, the calculations showed an average trapping energy of ~ 0.35 eV and ~ 0.49 eV for the double-electron and double-hole traps, respectively.

The one-electron deep trap identified in the GST-225 model systems creates a deep potential well in the amorphous structure. The modelling of double-electron traps shows that this potential well can accommodate two electrons at the same site, since the second extra electron is localized on the same structural environment as the first trapped electron. However, it seems that, compared to the one-electron system, there is significant further atomic relaxation in the structural pattern hosting the trap when the second electron is added. This is highlighted in Fig. 5, where the interatomic distances and the bond angles of the atomic species in the 5-membered chain-like structure, hosting two trapped electrons, undergo pronounced structural changes. We note that, for the one-electron trap, which is a doublet state (*i.e.* odd number of electrons), the spin-density distribution has been used to highlight the atomic structure where the electron is trapped (Fig. 5a), whereas for the two-electron trap, which is a singlet state (*i.e.* even number of electrons), the corresponding KS orbital is shown for visualization of the relevant trapping environment in the amorphous model (Fig. 5b).

The axial, almost-linear, triatomic configurations in the defective octahedral-like sites have been considered to be of significant importance regarding three-centre, four-electron bonding in amorphous chalcogenide materials.[57] Recently, the occurrence of such sites in phase-change memory materials was discussed in terms of hyperbonding.[58,59] These near-linear atomic geometries in amorphous GST-225 are the most polarizable, and thereby, potentially, are the most susceptible to bond breaking. In addition, after trapping of two electrons in the same structural environment, the energy barrier for breaking one such Ge/Sb–Te bond is reduced.

Atomic rearrangements related to bond breaking within the amorphous network have been suggested as being responsible for the structural relaxation of amorphous phase-change materials.[20–23,60] Moreover, very recently, we demonstrated that

Open Access Article. Published on 06 April 2022. Downloaded on 4/8/2022 12:18:25 PM.
This article is licensed under a Creative Commons Attribution 3.0 Unported Licence.

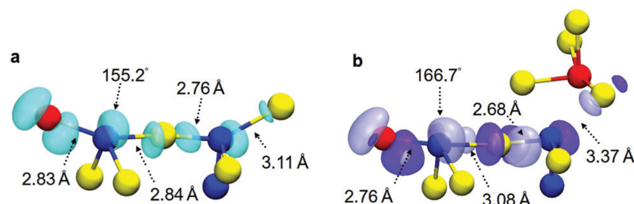

Fig. 5 (a) Spin-density distribution and atomic geometry of the one-electron trap in a GST-225 glass model (#25 from ref. 31). The extra electron is localized on a Te–Ge–Te–Ge–Sb chain-like structure. The iso-value of the spin density (cyan iso-surface) is equal to 0.002 e $Å^{-3}$. (b) Configuration of the two-electron trap in the same amorphous model. The coloured iso-surfaces correspond to the occupied Kohn–Sham state of the double-electron system, with iso-values equal to +0.02 (dark-blue) and −0.02 e $Å^{-3}$ (light-blue). In both cases, Ge atoms are blue, Sb are red, and Te are yellow. The bond lengths and bond angles (indicated by arrows) for the atoms involved in the chain motif that hosts the extra electrons show that the localization of the second trapped electron causes significant atomic relaxation.

the application of a sufficiently high homogeneous external electric field induces atomic relaxations of the amorphous structure, leading to structural modifications of local environments associated with defect-related localized states.[61] In particular, we illustrated an electric-field-induced breaking of the weak, polarizable bonds in 5-coordinated Ge atoms within the GST-225 amorphous structure, which results in an ''engineered'' (*i.e.* without thermal annealing) annihilation of mid-gap defect electronic states and the subsequent structural relaxation of the glassy model system.[61]

The stretching and breaking of the axial bonds in near-linear triatomic configurations, that form chain-like structural motifs and host the extra charges inside the modelled structures, is illustrated through two examples, for one- and two-electron traps in Fig. 6a, and for one- and two-hole traps in Fig. 6b. The initial stage of this procedure is the occurrence of a wide Te–Ge/Sb–Te angle of the ''see-saw'' 4-coordinated structure, which corresponds to an intrinsic electron/hole trap in the neutral GST-225 amorphous models. After electron/hole injection, the extra charge is trapped in these atomic environments and the localization causes bond stretching for some of the axial bonds. The addition of the second electron/hole and the subsequent localization on the same structural site leads to further stretching of these (long) bonds, which can result in bond breaking, as demonstrated in Fig. 6 for electron and hole trapping, respectively. It is noted that, in this analysis, bond formation is considered to occur between two nearby atoms if their interatomic distance is shorter than or equal to 3.2 Å. A similar weakening of

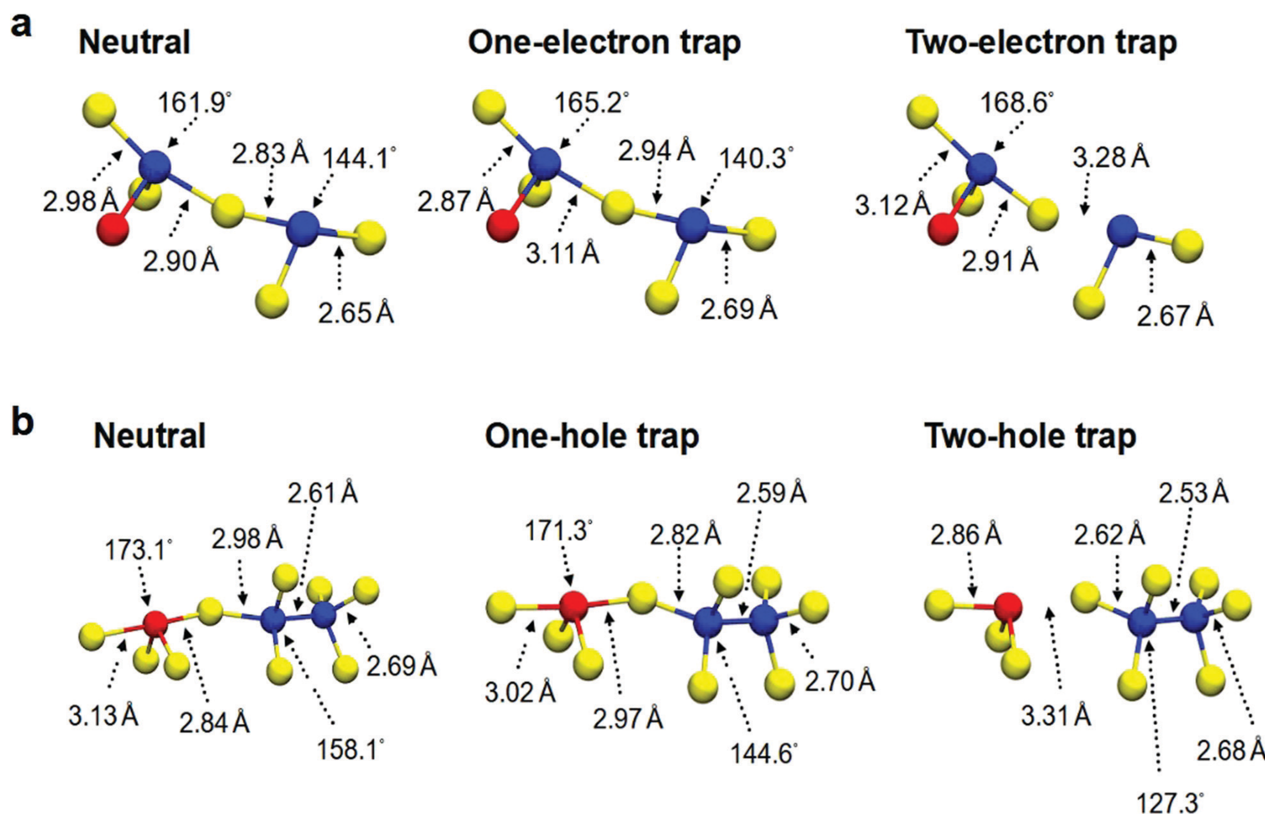

Fig. 6 (a) The atomistic structure of the chain-like environment where the first and second electrons are trapped in one of the simulated GST-225 structures (#19 from ref. 31). Electron injection and localization of the extra electrons in the intrinsic trap environment results in a widening of a Te–Ge–Te angle, bond stretching and finally breaking of a Ge–Te bond. (b) The atomistic structure of the chain-like environment where the first and second holes are trapped in one of the amorphous GST-225 models (#21 from ref. 31). Localization of two holes in the intrinsic trap environment leads to stretching and breaking of an axial bond between Sb and Te atoms in a ''see-saw'' 4-coordinated geometry. In both cases, Ge atoms are blue, Sb are red, and Te are yellow.

Open Access Article. Published on 06 April 2022. Downloaded on 4/8/2022 12:18:25 PM.
This article is licensed under a Creative Commons Attribution 3.0 Unported Licence.

atomic bonds due to charge trapping has been reported in amorphous SiO_2, where structural units with wide O–Si–O angles in $[SiO_4]$ tetrahedra can trap two extra electrons.[55]

4. Conclusions

Our first-principles simulations show that excess electrons and holes are spontaneously trapped in amorphous GST-225, creating charge-trapping centres in the band gap of the glassy material. Hybrid-DFT calculations were employed to optimize the geometry of an ensemble of amorphous models after electron/hole injection, and to calculate their electronic structures for identifying the structural fingerprint of charge trapping inside the glass network. The calculations demonstrate that spontaneous electron- and hole-trapping events are energetically favourable in amorphous GST-225. One-electron traps produce deep occupied states in the band gap, located at $\sim$0.58 eV below the bottom of the conduction band, while one-hole traps lead to the creation of unoccupied states around midgap. The intrinsic defective octahedral Ge and Sb sites inside the amorphous GST-225 network have been found to be responsible for the charge trapping. The almost-linear triatomic environments from the axial bonds in ''see-saw'' 4-coordinated or 5-coordinated defective-octahedral configurations correspond to the atomic geometries where the extra electrons and holes are trapped. 5-membered chain-like structures comprised of two connected triads have been also identified as potential charge-trapping sites. Moreover, trapping environments with a similar geometric nature have been observed in the as-deposited model structure of GST-225, even though the presence of tetrahedral Ge atoms is predominant within the amorphous network. This highlights the prevailing relevance of the defective octahedral atomic geometries in the charge-trapping processes.

Interestingly, the local atomic structure of the charge-trapping centres identified in our glassy telluride (GST-225) models is different than the negative-U coordination defects considered to be involved in shallow band-tail traps in sulphide- and selenide-based chalcogenide glasses,[62–64] where the concentration of potential trapping sites is also much lower.[65] Recently, hybrid-DFT electronic-structure calculations showed that 1- and 3-coordinated Se atoms, forming an intimate valence alternation pair (IVAP), participate in the spatial localization of the HOMO electronic state at the top of the valence band in an ''as-deposited'' model of amorphous Se.[66] Such IVAPs have also been suggested experimentally to serve as electron and hole recombination centres in glassy Se.[67]

The simulated trapping centres have a wide range of ionization energies, including relatively low values, suggesting that thermal release of the trapped electrons and holes would be feasible during the memory device operation, and also attainable over a long period of time. This observation, together with the calculated energy levels of the traps in the band gap of the glass (one-electron traps close to the top of the valence band; one-hole traps around midgap) supports a potential electronic mechanism for resistance drift in amorphous phase-change memory materials, where de-trapping of charge carriers and subsequent recombination is involved, following electron/hole injection during the *RESET* voltage pulse.[26] Moreover, photo-excitation experiments point to such an electronic component in the time-dependent resistance-drift, where trapping and de-trapping of electrons and holes, at low temperatures, can give rise to modifications in the current–voltage characteristics.[25]

The calculations show that trapping of two electrons and holes can form deeper states in the band gap. It was found that a second electron can be trapped at the same intrinsic chain-like structures, resulting in weakening and potential breaking of the axial polarizable bonds in the defective octahedral-like sites. This observation suggests that electron and hole trapping can create an athermal bond-breaking pathway of the chemically ordered connected triads within the amorphous network of GST-225, by reducing the barrier for Ge/Sb–Te bond breaking.

Heating up an amorphous GST-225 model with trapped electrons/holes by performing a MD simulation at finite temperatures is a potential follow-up study to investigate the possibility of a thermal release of trapped electrons within the (albeit necessarily short) time scale of the simulation. Also, this can enable the quantitative comparison of the dynamics of the de-trapping with the temperature-dependent onset of resistance drift.[24] Modelling vertical excitations with ground-state DFT is another possible extension of the present work. The relaxed geometry of the lowest-triplet-excited state can be quenched electronically back to the singlet state, and the geometry of the amorphous structure then re-optimized. Such calculations would give information on the stability of the glass structure against the recombination of electrons and holes. Finally, optical excitations of trapped electrons in the band gap can be studied by performing MD simulations with time-dependent DFT in future investigations.

Understanding electron- and hole-trapping processes in amorphous phase-change memory materials is imperative with respect to the device operation. The calculations presented in this study provide an atomistic description of the electronic and structural aspects related to charge trapping. The results demonstrate the inherent nature of electron and hole trapping in amorphous GST-225, while they also reveal the atomic configurations that can capture extra electrons/holes inside the glass network. The overall findings can have significant ramifications for the programming operation in PCRAM devices.

Author contributions

K. K. designed and developed the concept of the research study. K. K. carried out the simulations, analysed the results and constructed the figures. K. K., S. R. E. and J. A. interpreted the data. K. K., S. R. E. and J. A. wrote the manuscript. All authors have given approval to the final version of the manuscript.

Conflicts of interest

There are no conflicts to declare.

Open Access Article. Published on 06 April 2022. Downloaded on 4/8/2022 12:18:25 PM.
This article is licensed under a Creative Commons Attribution 3.0 Unported Licence.

This journal is © The Royal Society of Chemistry 2022

Acknowledgements

K. K. and J. A. acknowledge financial support from the Academy of Finland project No. 322832 "NANOIONICS". *Via* our membership of the UK's HEC Materials Chemistry Consortium, which is funded by EPSRC (EP/L000202, EP/R029431), this work used the ARCHER UK National Supercomputing Service (**https://www.archer.ac.uk**). The authors wish to acknowledge the CSC – IT Center for Science, Finland, for computational resources.

Open Access Article. Published on 06 April 2022. Downloaded on 4/8/2022 12:18:25 PM.
This article is licensed under a Creative Commons Attribution 3.0 Unported Licence.

References

1 N. F. Mott, E. A. Davis and R. A. Street, *Philos. Mag.*, 1975, **32**, 961–996.
2 J. Strand, M. Kaviani, V. V. Afanas'ev, J. G. Lisoni and A. L. Shluger, *Nanotechnology*, 2018, **29**, 125703.
3 J. Strand, M. Kaviani, D. Gao, A. M. El-Sayed, V. V. Afanas'ev and A. L. Shluger, *J. Phys.: Condens. Matter*, 2018, **30**, 233001.
4 A. M. El-Sayed, M. B. Watkins, V. V. Afanas'ev and A. L. Shluger, *Phys. Rev. B*, 2014, **89**, 125201.
5 K. Konstantinou, D. M. Duffy and A. L. Shluger, *Phys. Rev. B*, 2016, **94**, 174202.
6 O. A. Dicks and A. L. Shluger, *J. Phys.: Condens. Matter*, 2017, **29**, 314005.
7 J. Strand, O. A. Dicks, M. Kaviani and A. L. Shluger, *Microelectron. Eng.*, 2017, **178**, 235–239.
8 D. Mora-Fonz and A. L. Shluger, *Adv. Electron. Mater.*, 2020, **6**, 1900760.
9 D. Mora-Fonz, M. Kaviani and A. L. Shluger, *Phys. Rev. B*, 2020, **102**, 054205.
10 A. M. El-Sayed, M. B. Watkins, A. L. Shluger and V. V. Afanas'ev, *Microelectron. Eng.*, 2013, **109**, 68–71.
11 M. Kaviani, J. Strand, V. V. Afanas'ev and A. L. Shluger, *Phys. Rev. B*, 2016, **94**, 020103(R).
12 R. Bez and A. Pirovano, *Mater. Sci. Semicond. Process.*, 2004, **7**, 349.
13 S. Raoux, W. Welnic and D. Ielmini, *Chem. Rev.*, 2010, **110**, 240.
14 D. Adler, M. S. Shur, M. Silver and S. R. Ovshinsky, *J. Appl. Phys.*, 1980, **51**, 3289.
15 A. Redaelli, A. Pirovano, A. Benvenuti and A. L. Lacaita, *J. Appl. Phys.*, 2008, **103**, 111101.
16 A. Pirovano, A. L. Lacaita, F. Pellizzer, S. A. Kostylev, A. Benvenuti and R. Bez, *IEEE Trans. Electron Devices*, 2004, **51**, 714.
17 P. Noé, C. Vallée, F. Hippert, F. Fillot and J. Y. Raty, *Semicond. Sci. Technol.*, 2018, **33**, 013002.
18 D. Ielmini, S. Lavizzari, D. Sharma and A. L. Lacaita, *Appl. Phys. Lett.*, 2008, **92**, 193511.
19 M. Boniardi and D. Ielmini, *Appl. Phys. Lett.*, 2011, **98**, 243506.
20 J. Y. Raty, W. Zhang, J. Luckas, C. Chen, R. Mazzarello, C. Bichara and M. Wuttig, *Nat. Commun.*, 2015, **6**, 7467.
21 S. Gabardi, S. Caravati, G. C. Sosso, J. Behler and M. Bernasconi, *Phys. Rev. B*, 2015, **92**, 054201.
22 F. Zipoli, D. Krebs and A. Curioni, *Phys. Rev. B*, 2016, **93**, 115201.
23 M. Le Gallo, D. Krebs, F. Zipoli, M. Salinga and A. Sebastian, *Adv. Electron. Mater.*, 2018, **4**, 1700627.
24 B. Kersting, S. Ghazi Sarwat, M. Le Gallo, K. Brew, S. Walfort, N. Saulnier, M. Salinga and A. Sebastian, *Adv. Funct. Mater.*, 2021, **31**, 2104422.
25 R. S. Khan, F. Dirisaglik, A. Gokirmak and H. Silva, *Appl. Phys. Lett.*, 2020, **116**, 253501.
26 S. R. Elliott, *J. Phys. D: Appl. Phys.*, 2020, **53**, 214002.
27 J. Luckas, D. Krebs, M. Salinga, M. Wuttig and C. Longeaud, *Phys. Status Solidi C*, 2010, **7**, 852.
28 J. Luckas, D. Krebs, S. Grothe, J. Klomfaß, R. Carius, C. Longeaud and M. Wuttig, *J. Mater. Res.*, 2013, **28**, 1139.
29 M. Kaes and M. Salinga, *Sci. Rep.*, 2016, **6**, 31699.
30 S. Caravati, M. Bernasconi, T. D. Kühne, M. Krack and M. Parrinello, *J. Phys.: Condens. Matter*, 2009, **21**, 255501.
31 K. Konstantinou, F. C. Mocanu, T. H. Lee and S. R. Elliott, *Nat. Commun.*, 2019, **10**, 3065.
32 H. Li and J. Robertson, *Appl. Phys. Lett.*, 2020, **116**, 052103.
33 F. C. Mocanu, K. Konstantinou, J. Mavračić and S. R. Elliott, *Phys. Status Solidi RRL*, 2021, **15**, 2000485.
34 F. C. Mocanu, K. Konstantinou, T. H. Lee, N. Bernstein, V. L. Deringer, G. Csányi and S. R. Elliott, *J. Phys. Chem. B*, 2018, **122**, 8998.
35 J. Akola and R. O. Jones, *Phys. Rev. B*, 2007, **76**, 235201.
36 J. Akola, J. Larrucea and R. O. Jones, *Phys. Rev. B*, 2011, **83**, 094113.
37 J. VandeVondele, M. Krack, F. Mohamed, M. Parrinello, T. Chassaing and J. Hutter, *Comput. Phys. Commun.*, 2005, **167**, 103.
38 G. Lippert, J. Hutter and M. Parrinello, *Mol. Phys.*, 1997, **92**, 477.
39 J. VandeVondele and J. Hutter, *J. Chem. Phys.*, 2007, **127**, 114105.
40 S. Goedecker, M. Teter and J. Hutter, *Phys. Rev. B*, 1996, **54**, 1703.
41 M. Guidon, J. Hutter and J. VandeVondele, *J. Chem. Theory Comput.*, 2009, **5**, 3010.
42 K. Konstantinou, T. H. Lee, F. C. Mocanu and S. R. Elliott, *Proc. Natl. Acad. Sci. U. S. A.*, 2018, **115**, 5353.
43 M. Guidon, J. Hutter and J. VandeVondele, *J. Chem. Theory Comput.*, 2010, **6**, 2348.
44 B. S. Lee, J. R. Abelson, S. G. Bishop, D. H. Kang, B. K. Cheong and K. B. Kim, *J. Appl. Phys.*, 2005, **97**, 093509.
45 T. Kato and K. Tanaka, *Jpn. J. Appl. Phys.*, 2005, **44**, 7340.
46 S. Caravati, M. Bernasconi, T. D. Kühne, M. Krack and M. Parrinello, *Appl. Phys. Lett.*, 2007, **91**, 171906.
47 J. Akola and R. O. Jones, *J. Phys.: Condens. Matter*, 2008, **20**, 465103.
48 T. H. Lee and S. R. Elliott, *Adv. Mater.*, 2017, **29**, 1700814.
49 S. Caravati, M. Bernasconi and M. Parrinello, *Phys. Rev. B*, 2010, **81**, 014201.
50 K. Konstantinou, J. Mavračić, F. C. Mocanu and S. R. Elliott, *Phys. Status Solidi B*, 2021, **258**, 2000416.
51 G. C. Sosso, G. Miceli, S. Caravati, J. Behler and M. Bernasconi, *Phys. Rev. B*, 2012, **85**, 174103.

52 F. C. Mocanu, K. Konstantinou and S. R. Elliott, *J. Phys. D: Appl. Phys.*, 2020, **53**, 244002.
53 N.-K. Chen, X.-B. Li, X.-P. Wang, W. Q. Tian, S. Zhang and H.-B. Sun, *Acta Mater.*, 2018, **143**, 102–106.
54 S. Chen and L.-W. Wang, *Phys. Rev. B*, 2014, **89**, 014109.
55 D. Z. Gao, A. M. El-Sayed and A. L. Shluger, *Nanotechnology*, 2016, **27**, 505207.
56 E. S. Fois, A. Selloni, M. Parrinello and R. Car, *J. Phys. Chem.*, 1988, **92**, 3268–3273.
57 A. V. Kolobov, P. Fons, J. Tominaga and S. R. Ovshinsky, *Phys. Rev. B*, 2013, **87**, 165206.
58 T. H. Lee and S. R. Elliott, *Adv. Mater.*, 2020, **32**, 2000340.
59 T. H. Lee and S. R. Elliott, *Phys. Status Solidi RRL*, 2021, **15**, 2000516.
60 P. Fantini, M. Ferro, A. Calderoni and S. Brazzelli, *Appl. Phys. Lett.*, 2012, **100**, 213506.
61 K. Konstantinou, F. C. Mocanu, J. Akola and S. R. Elliott, *Acta Mater.*, 2022, **223**, 117465.
62 R. A. Street and N. F. Mott, *Phys. Rev. Lett.*, 1975, **35**, 1293.
63 M. Kastner, D. Adler and H. Fritzsche, *Phys. Rev. Lett.*, 1976, **37**, 1504.
64 M. L. Benkhedir, M. S. Aida and G. J. Adriaenssens, *J. Non-Cryst. Solids*, 2004, **344**, 193.
65 D. Adler and E. J. Yoffa, *Phys. Rev. Lett.*, 1976, **36**, 1197.
66 J. Kalikka, K. Konstantinou, J. Akola and R. O. Jones, *J. Phys.: Condens. Matter*, 2021, **33**, 445401.
67 J. Jacobs, G. Belev, A. Brookfield, F. Tuna, S. Kasap and R. J. Curry, *J. Mater. Sci.: Mater. Electron.*, 2020, **31**, 15489.

Open Access Article. Published on 06 April 2022. Downloaded on 4/8/2022 12:18:25 PM.
This article is licensed under a Creative Commons Attribution 3.0 Unported Licence.

 This journal is © The Royal Society of Chemistry 2022